Programmed Emission Transformations: Negative-to-Positive Patterning Using the Decay-to-Recovery Behavior of Quantum Dots

*Sidney T. Malak, Marcus J. Smith, Young Jun Yoon, Chun Hao Lin, Jaehan Jung, Zhiqun Lin, and Vladimir V. Tsukruk**

Positive and negative photoluminescent photopattern contrasts arising from intrinsic modification of quantum dot (QD) emission (decay or recovery) upon exposure to light are reported. The ability to fabricate a variety of photopattern types using a single type of quantum dot is due to a two-step decay-to-recovery evolution upon light exposure. It is shown that high-contrast photopatterns spanning mm^2 areas can be fabricated within seconds with a facile one-step process, representing a drastic reduction in the time required to develop an emissive pattern in a QD-polymer film (from hours to seconds). Furthermore, the controlled light exposure allows for a programmed transformation of the emissive pattern contrast, with a reversal of the bright/dark regions of the QD-polymer photopattern demonstrated. Finally, it is shown that the photopatterns can be stored over a period of time and then "recharged" using simple light exposure to partially recover the intensity and contrast of aged photopatterns. The outlined patterning strategies open up new pathways for facile, one-step parallel fabrication of anti-counterfeiting emitting labels and light sensors, as well as for gain-loss parity-time systems where an emission contrast is required but where physical patterning may not be appropriate.

1. Introduction

The area of photonic materials and systems has benefited greatly from the development of nanoparticles that display highly controlled light emission, scattering, and absorption properties.[1–4] The great versatility of nanoparticles is due in large part to the tunable nature of their properties, with changes in size, shape, coupling, and orientation leading to large controllable changes in the optical properties.[5–8] Quantum dots (QDs) are a particularly interesting nanostructure for applications that require optical emission in the visible or near-infrared spectrum. These small (D < 10 nm) semiconducting nanoparticles exhibit size-dependent broadband absorption and narrowband photoluminescence (PL) (full-width half-maximum (FWHM) below 40 nm) due to quantum confinement of the exciton.[9–11] Many synthesis approaches have been developed for different QD architectures, including core,[12] core–shell,[13,14] alloyed core–shell,[15] and even core–shell–shell QDs,[16] which offer a range of optical characteristics. Not surprisingly, the intrinsic properties of QDs and the wide variety of QDs available have led to their implementation in a number of applications, including imaging/labeling/sensing in biological investigations,[17] light-emitting diodes (LEDs),[18] solar cells,[19,20] quantum computing,[21] and, more recently, lasers and optical gain media.[22–24]

In addition, the application of nanotechnology for controlled light–matter interactions has been augmented by the variety of micro- and nanoscale patterning approaches that have been developed, including techniques like electron- and photolithography,[25] soft lithographies,[26,27] inkjet printing,[28] and molding and printing.[29] One of the unifying principles of these approaches is that patterns are created by adding, removing, or rearranging material during a multi-step fabrication procedure. Less investigation has been done on "non-physical" patterning approaches like spectral photopatterning, which creates patterns by modifying the emission efficiency of quantum dots in specific areas of the film without physically modifying the film.[30–33] The modification of QD emission efficiency is due to intrinsic modification of the exciton relaxation pathways within the QD, so no physical deposition or removal of material is required to impart an emission pattern in a spectral photopattern. The non-physical aspect of spectral photopatterning is in sharp contrast to the traditional micro- and nanoscale physical patterning techniques. For this reason, spectral photopatterning could be very useful in areas such as photonic parity-time systems that require periodic modulation of optical gain and loss with no corresponding change in

S. T. Malak, M. J. Smith, Y. J. Yoon,
C. H. Lin, Dr. J. Jung, Prof. Z. Lin, Prof. V. V. Tsukruk
School of Materials Science and Engineering
Georgia Institute of Technology
Atlanta, GA 30332, USA
E-mail: vladimir@mse.gatech.edu
M. J. Smith
Aerospace Systems Directorate
Air Force Research Laboratory
Wright-Patterson Air Force Base
OH 45433, USA

DOI: 10.1002/adom.201600509

the real refractive index (which can limit the applicability of more traditional physical patterning approaches).[34,35] In addition, spectral photopatterning has potential in overcoming the obstacles associated with the scaling-up of nano/microscale patterned systems because pattern contrast can be imparted and controlled via simple remote light exposure.

The spectral photopatterning approach requires optically emitting nanostructures that exhibit a change in emission (an increase or decrease of intensity or a spectral shift) when exposed to light.[30–33] Although quantum dots are typically used in photopatterning, other materials like conjugated polymers, dyes, and nanostructures can also be used if their emission changes in response to light. Photopatterning requires the deliberate introduction of optical nanostructures with unstable PL into a system, which is generally considered detrimental in optical systems since the emission intensity, position, and FWHM can be intimately tied to the functioning of the device. Quantum dots can be synthesized to have unstable emission (while maintaining a narrow emission band and strong photoluminescence in the visible spectrum),[30–33] making them promising candidates for photopatterning. Previous QD photopatterning studies have almost exclusively exploited QDs that undergo an increase in emission when exposed to light and have required up to 24–72 hours to develop a photopattern.[30,31,36] However, QDs can show complex changes in their PL emission when exposed to light, including an increase, decrease, or spectral shift depending on their synthesis, surrounding environment, and exposure conditions.[37,38] The underlying mechanisms behind these changes in QD emission intensity include degradation of emission quenchers,[30] photoactivation,[31,39] photoelectrification,[40,41] photoionization,[42] as well as the underlying substrate.[43,44] All of these changes and mechanisms can be taken advantage of to develop new strategies for photopatterning.

In this work, we introduce novel approaches for developing pre-determined formations of positive and negative contrast emissive patterns in QD-polymer films. The resulting photopatterns have strong emission contrast, microscale resolution, and can span macroscopic lateral areas. Furthermore, the contrast of a negative pattern can be transformed to a positive pattern, a feat not possible using traditional lithographic approaches. The outlined strategies rely on the intrinsic modification of QD emission that occurs when exposed to light, with multiple pattern strategies possible due to the unique decay-to-recovery evolution of the emission over intermediate timescales (seconds to minutes). However, the outlined strategies are not limited to quantum dot systems, instead being compatible with any material (dye, conjugated polymer, nanoparticle) that undergoes a change of emission (intensity or color) when exposed to light. These novel approaches offer a complementary microscale patterning option to traditional lithographies that require the addition or removal of material and chemical treatments to provide pattern contrast.

2. Results and Discussion

2.1. QD Properties and PL Emission Evolution

The photoluminescence of the CdSe/ZnS QDs is in the green region and has a full-width half-maximum near 40 nm (**Figure 1**). The evolution of PL intensity for the QD-polymer film when exposed to light has two distinct steps: a fast and large decay on the order of seconds followed by a slower partial recovery on the order of many minutes (Figure 1a,b, log scales). A large decrease of intensity occurs within the first seconds of light exposure while the spectral center and FWHM remain nearly constant (Figure S1, Supporting Information).

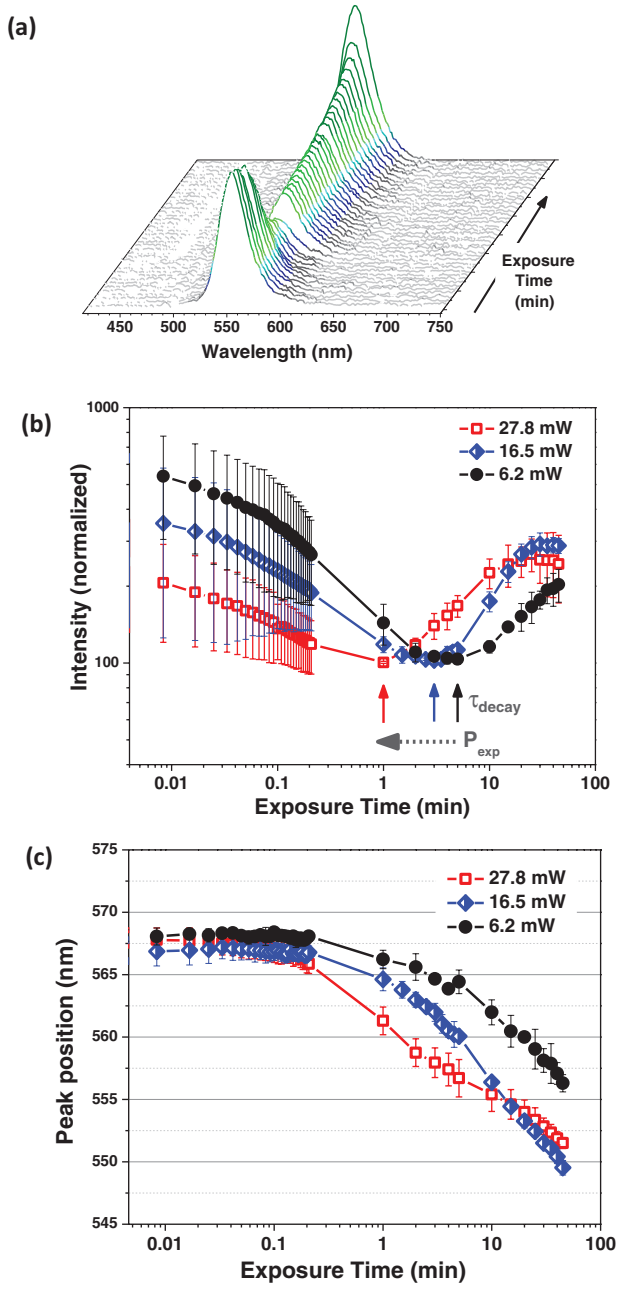

Figure 1. The photoluminescence intensity and spectral position of QD-polymer films change when exposed to light. a) Waterfall plot of the photoluminescence spectrum when exposed to light (470 nm) over a period of 45 min. Peak fitting of the photoluminescence spectra show that the b) intensity (normalized to minimum value) and c) spectral center shift under continuous light exposure of different incident power.

This decay-to-recovery behavior occurs over a range of exposure powers with higher exposure power reducing the time required for the PL intensity to reach its minimum value (Figure 1b). Note it appears that lower exposure power leads to a greater decrease of intensity within the first seconds of light exposure. However, this trend is likely due to the higher exposure power decaying the PL so quickly that it cannot be measured by the instrument in the first moments of exposure (while low power exposure causes a slower PL decay rate that can be tracked more easily). For these reasons, the PL intensity data were normalized against the lowest emission value, which occurs over longer time scales (minutes) and can be accurately measured.

The time-to-minimum intensity (or the time required to enter the recovery stage) shows a clear dependence on exposure power for the power range examined, with higher exposure power reducing the amount of time required to enter the recovery stage. This trend suggests that the physical mechanisms causing the decay-to-recovery behavior is controlled by the number of incident photons. In contrast, the spectral center of the PL peak undergoes a blue-shift over the entire exposure period (Figure 1c), indicating an increase in quantum confinement of the exciton throughout the process. The FWHM of the emission shows no clear trend with exposure power (Figure S2, Supporting Information).

Multiple mechanisms might control the decay-to-recovery behavior of emission intensity, with all likely involving changes to surface passivation of the quantum dot since surface passivation is often cited as strongly affecting quantum yield.[14,45] In this case, a decay of photoluminescence can be attributed to a reduction of surface passivation of the QD core by the shell. More specifically, the sharp core–shell interface of the QDs and lattice mismatch between CdSe and ZnS (12%) cause voids and defects to form due to lattice strain.[15,46,47] Before exposure to light, the sharp core–shell CdSe/ZnS interface is in a metastable state. Upon light exposure, the interface is disrupted by the formation of surface oxides and the potential rearrangement of ZnS atoms which reduces surface passivation (at least initially).[14] In addition, photooxidation/corrosion of the ZnS shell has been shown to form surface quenching states that reduce quantum yield and cause a spectral blue shift.[38,48] On the other hand, previous reports have attributed a recovery of intensity upon light exposure to a variety of mechanisms including photoinduced surface annealing or restructuring,[49] interfacial alloying of the core–shell interface,[15,50] or light-induced H_2O passivation of surface defects.[38] In this case, it is likely a combination of photoinduced surface annealing and restructuring of the QD surface (irreversible) and light-induced H_2O defect passivation (reversible) because the PL recovery is partially reversible (discussed later).

It is important to recognize the importance of the very fast decay of emission (within seconds) after light exposure for materials patterning. The high rate of this decay can be difficult to observe due to it being in an intermediate timescale (seconds) that is much slower than intrinsic exciton dynamic lifetimes (picosecond to nanosecond) but much faster than typical steady state PL measurements (minutes). Therefore, this behavior has likely been not accounted for in QD stability studies that measured emission using much longer timesteps (on the order of minutes).

2.2. Photopatterning with Light Exposure

The general approach for spectral photopatterning involves the selective exposure of specific regions of a film composed of light-emitting structures that undergo a change of emission intensity or spectral position when exposed to light (**Figure 2**). In this study, a simple copper TEM grid serves as the photomask to provide selective exposure of specific

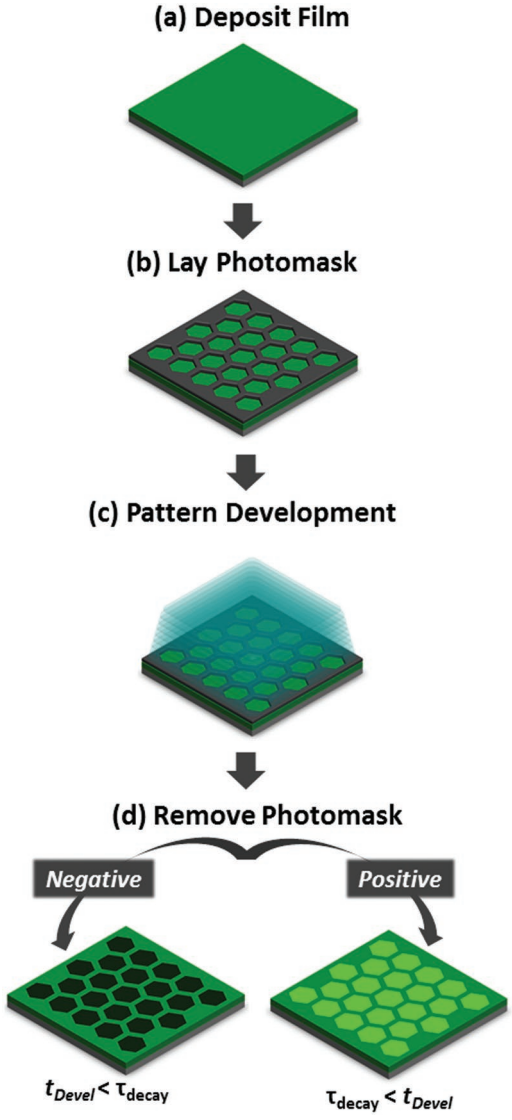

Figure 2. Schematic of the two most basic photopatterning approaches in this study: a) A QD-polymer film is deposited on a substrate and b) a photomask is laid on top. c) The system is exposed to light to develop the photopattern and d) then the mask is removed to reveal the photopattern. The type of photopattern (negative or positive) depends on whether the development time (t_{Devel}) is less than or greater than the time-to-minimum (τ_{decay}).

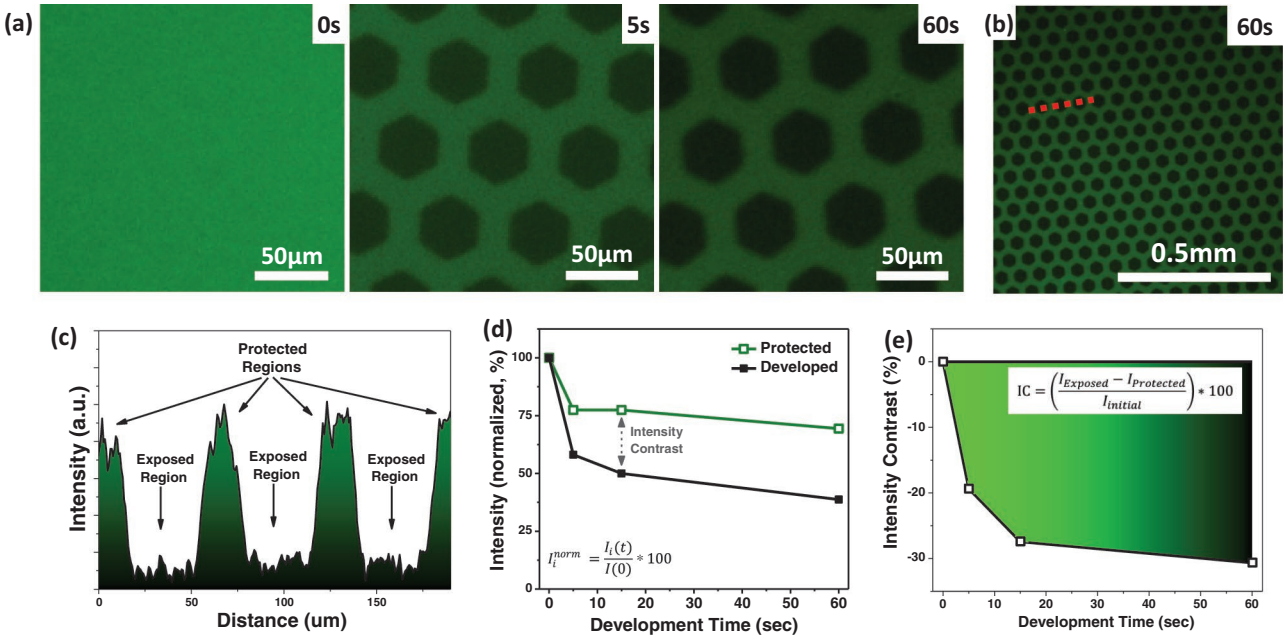

Figure 3. Negative photopatterning (NP) occurs if the QD-polymer film is developed for a time period less than the characteristic PL time-to-minimum (i.e., $t_{devel} < \tau_{decay}$). a) PL images of a negative photopattern at different stages of pattern development (developed using light of 470 nm, 5.7 mW). b) Photoluminescence image of a negative photopattern spanning a large area (mm^2). c) PL intensity cross section of a negative photopattern PL image (60 s development pattern). d) Intensity of the protected and developed regions of the photopattern and e) the corresponding intensity contrast IC for different development times.

regions of the composite quantum dot-polymer (QD-polymer) film. However, the only constraint of the photomask is that it is opaque to the light wavelength used to develop the photopattern. The resulting emissive pattern is due to the intrinsic modification of QD emission (intensity) due to light exposure; the pattern is not due to the addition or removal of material as in conventional photolithography and electron beam lithography. This is indeed confirmed by atomic force microscopy (AFM) and bright field imaging of photopatterned regions that show no physical modification of the film that could account for the PL pattern (Figures S3 and S4, Supporting Information).

Nearly all previous demonstrations of spectral photopatterning were of positive photopatterns, meaning the regions of the film exposed to light undergo an increase in their emission and therefore are the highest intensity regions. However, the photopatterning approach can be extended beyond positive photopatterns by using QDs that undergo the complex decay-to-recovery intensity behavior of the CdSe/ZnS QDs examined in this study (Figure 1b).

In this situation, both positive and negative contrast patterns can be fabricated by controlling the amount of light exposure time. Specifically, negative contrast patterns can be fabricated using a development time shorter than the time-to-minimum period (τ_{decay}), while positive patterns can be fabricated using development times longer than τ_{decay} (without changing the overall setup) (Figure 2d). In short, the τ_{decay} defines the transition between negative and positive photopattern development, and τ_{decay} can be controlled explicitly by the exposure power (Figure 1b). The following section outlines these points in detail.

2.3. Negative Photopatterning

The negative photopatterning approach yields a photopattern where the regions of the QD-polymer film exposed to the development light have a lower PL intensity than the regions protected by the photomask (Figure 2). A negative photopattern is fabricated by developing the film for a time (t_{devel}) shorter than the QD time-to-minimum period (i.e., $t_{devel} < \tau_{decay}$) since the exposed QDs are still within the decay phase of their PL evolution (Figure 1a,b).

The negative photopatterns display a clear intensity contrast (IC) between the exposed and protected regions of the film, which increases in magnitude as the development time approaches the τ_{decay} (**Figure 3**a). The photopattern corresponds closely to the photomask (Figure S5, Supporting Information) and is very uniform in terms of shape, size, and intensity over mm^2 lateral areas (Figure 3b). The IC between the exposed (dark) and protected (bright) regions of the negative photopattern is clearly visible from the PL cross sections (Figure 3c). Comparison of the intensity from the exposed ($I_{exposed}$) and protected ($I_{protected}$) regions, normalized against the intensity of the film before pattern development ($I_{Initial}$), shows that the exposed region experiences twice as much decay as the protected region (50% vs 25%) (Figure 3d). The intensity contrast of a photopattern, which indicates how distinct a pattern appears, is a critical parameter for evaluation and therefore should be quantified. Intensity contrast is therefore defined as

$$\mathrm{IC} = \left(\frac{I_{\mathrm{Exposed}} - I_{\mathrm{Protected}}}{I_{\mathrm{initial}}} \right) \times 100 \quad (1)$$

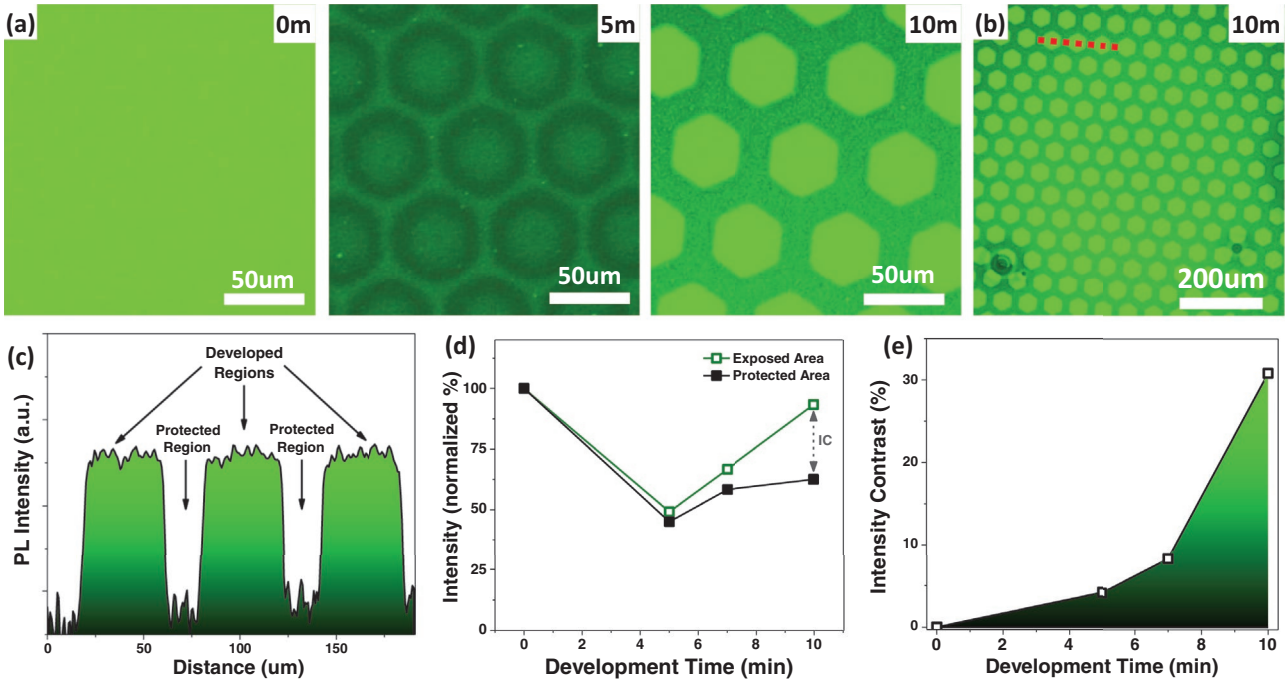

Figure 4. Positive contrast patterning (PP) occurs if the QD-polymer film is developed for a time period longer than the characteristic PL time-to-minimum (i.e., $\tau_{decay} < t_{devel}$). a) PL images of a positive photopattern at different stages of pattern development (developed using light of 470 nm, 34 mW). b) Photoluminescence image of a positive photopattern spanning a large area (mm^2). c) PL intensity cross section of a positive photopattern PL image (10 min development pattern). d) Intensity of the protected and developed regions of the photopattern and e) the corresponding intensity contrast for different development times.

According to this definition of intensity contrast, negative photopatterns have a negative intensity contrast since the developed regions of the photopattern have a lower intensity (they are darker) than the protected regions. Positive photopatterns have a positive IC which indicates the opposite scenario. Overall, we can conclude that the magnitude of intensity contrast is largest when there is a large difference of intensity between the developed regions of the pattern and the protected regions of the pattern.

In this demonstration of negative patterning, it is clear that the magnitude of IC increases as $t_{devel} \rightarrow \tau_{decay}$ (as expected), increasing from an IC of 0% at 0 s to −30% at 60 s of development (Figure 3e).

An attractive advantage of the negative photopatterning approach is that photopatterns with high contrast can be developed very quickly (<5 s) because of the rapid decay that occurs upon light exposure. In addition, because the τ_{decay} displays a negative trend with development power, the rate of pattern development can be controlled by exposure power. These patterns were developed significantly faster (more than 10 000 times) than some previous literature demonstrations (which often required 24–72 h) while maintaining spatial resolution (≈25 µm).[30,31] Spatial resolution in this case is dictated by the mask dimensions since the distances are much larger than the diffraction limit for 470 nm (<1 µm). In fact, demonstrations of higher resolution photopatterns using high-resolution TEM grids have been demonstrated[33] but were not the focus of this investigation. The substantial reduction in the time required to develop a high contrast photopattern stems from the fact that the fast PL decay mechanism provides the pattern contrast, whereas previous literature demonstrations used the degradation of quenchers or photoactivation to develop the pattern contrast (which are slower processes).[30,31]

2.4. Positive Photopatterning (PP)

The positive photopatterning approach yields a photopattern where the regions of the film exposed to the development light have a higher PL intensity than the regions protected by the photomask (Figure 2). A positive photopattern results if the pattern development time is longer than the decay period (i.e., $\tau_{decay} < t_{devel}$) since the exposed regions enter the recovery phase of their PL evolution (Figure 1b). Positive photopatterns require more time to develop ($t_{devel} \approx$ minutes) than negative photopatterns because the rate of PL recovery is slower than the rate of PL decay, but positive patterns tend to be very bright.

A demonstration of positive patterning is shown in **Figure 4**a. The areas exposed to light during the pattern development step are very bright while the protected regions are darker (positive intensity contrast). The photopattern is very uniform in terms of shape, size, and intensity over areas approaching mm^2 with a similar spatial resolution to negative photopatterning (Figure 4b). Cross sections of the PL image show a clear increase of PL intensity for the regions of the film exposed to light compared to the regions protected by the mask during the pattern development stage (Figure 4c,d). Tracking of PL intensity from the different regions of the pattern shows a positive intensity contrast that increases with development time and

eventually reaches a value of 30% at the longest development time (10 min) (Figure 4e).

It is interesting to note that at intermediate development times (5 min) a coronal pattern is formed with a high-intensity central region surrounded by a lower intensity corona. This effect arises due to low-intensity light bleeding (proximity effect) into the region surrounding the exposed hexagon region. The low intensity leads to decay of intensity but is not sufficiently strong to cause intensity recovery in the allotted time (Figure 4a and Figure S6, Supporting Information).

In this instance of positive photopatterning, dark field imaging does show some indication of the photopattern (Figure S7, Supporting Information). The exposed areas of the QD-polymer films scatter less light, which could be due to a reduction in the size of the QDs from oxidation that reduces their scattering cross section. The time required to fabricate these positive photopatterns is more than 100 times faster than previous demonstrations (from hours to minutes). This reduction results from the unstable core–shell composition.[30,31]

Overall, positive photopatterns exhibit higher PL intensity and better pattern stability than negative photopatterns because the pattern contrast is provided by the slower recovery step. When the entire positive photopattern is exposed to light, the protected regions undergo a rapid decay (as in the case of negative patterns). The rapid decay of the protected regions actually increases the pattern contrast since the difference of intensity between the high and low-intensity regions is now greater. Nevertheless, continued exposure eventually causes the protected regions to enter their recovery phase which does lead to a decrease in pattern contrast (shown later).

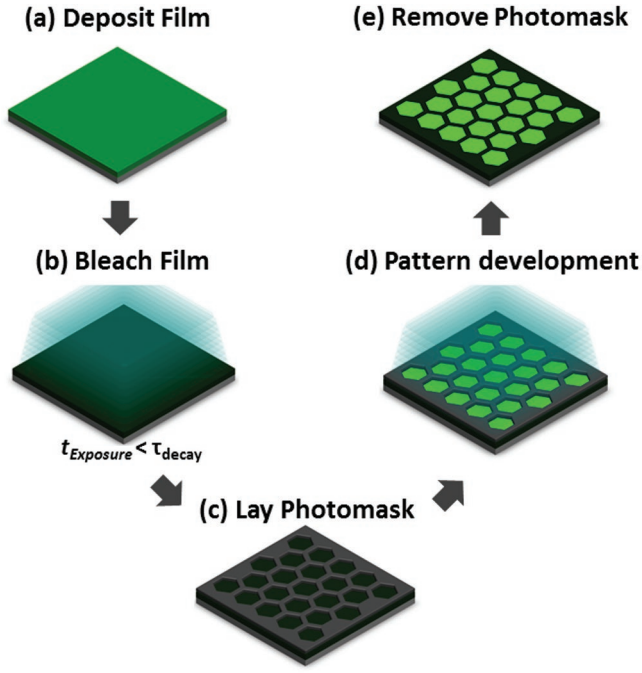

Figure 5. A positive photopatterning approach that can yield more stable photopatterns. This approach (preliminary decay-positive patterning, preD-PP) involves reducing the PL of the QD-polymer film before developing a positive photopattern. a,b) A QD-polymer film is exposed to light to reduce its PL to a near-minimum value. c,d) A photomask is laid on top and the system is exposed to light to develop the pattern. e) After removing the photomask, a positive photopattern is present.

2.5. Preliminary Decay-Positive Patterning (preD-PP)

More stable positive photopatterns can be fabricated by decaying the film to near its minimum intensity before performing the steps for positive patterning (**Figure 5**). The introduction of a preliminary decay step can improve pattern stability because all regions of the film have already experienced the fast decay step, essentially deactivating it. This means stray light exposure of the protected regions, which tends to reduce pattern stability, is less significant. Although this preD-PP approach incorporates an additional pre-decay step ($t_{devel} < \tau_{decay}$) before the positive patterning step , the resulting photopattern appears similar to the positive patterns shown previously.

These preD-PP patterns display a positive intensity contrast that corresponds closely to the mask and shows a similar development rate of intensity contrast to positive photopatterning (**Figure 6**a).

PL cross sections and intensity tracking show a clear positive intensity contrast between the developed and protected regions of the photopattern (Figure 6b,c). A maximum IC of 30% occurs at the longest development time (10 min). PL imaging using smaller time steps provides a more clear indication of how the pattern develops over a period of 10 min (Figure S8, Supporting Information). As mentioned, this preD-PP approach yields a positive photopattern similar to that obtained from the PP approach outlined previously, but exhibits better stability upon subsequent light exposure because all regions of the film have had their decay-step deactivated.

2.6. Negative-to-Positive Contrast Switching (N-P-CS)

The most intriguing discovery was that the approach explored here makes it possible to switch a negative photopattern to a positive photopattern (**Figure 7**).

This strategy, called N-P-CS, involves exposing an entire negative photopattern to light (no mask present) after the pattern has already been developed. Contrast switching from negative to positive occurs because the low-intensity and high-intensity regions of the QD-polymer film are at different stages of the decay-to-recovery evolution. For instance, the low-intensity regions of the negative photopattern have already undergone decay so further exposure to light causes these regions to enter the PL recovery step. On the other hand, the high-intensity regions of the negative photopattern have not undergone their decay step (since they were protected from the exposure light by the mask) so light exposure causes these regions to enter the rapid PL decay step.

A demonstration of this N-P-CS approach is shown in **Figure 8**a (Video S1, Supporting Information). A negative photopattern was first fabricated. Following this, the entire negative photopattern was exposed to light (470 nm, 23 mW) for 1 min or greater. Initially, the negative photopattern displays a large negative intensity contrast (0.4 s panel). However, upon continued

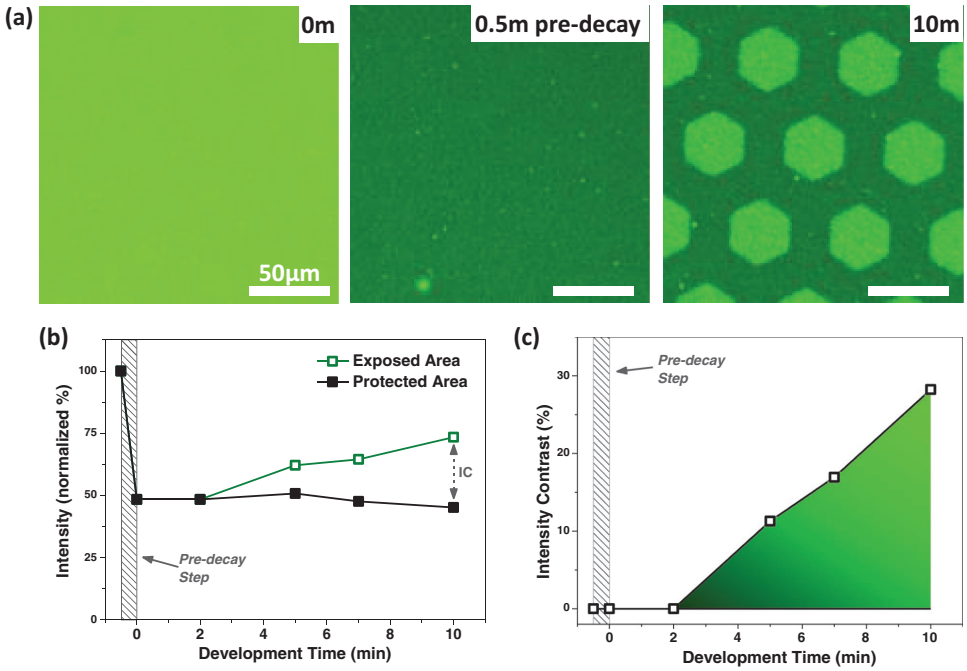

Figure 6. The preliminary decay-positive patterning (preD-PP) approach yields a stable positive photopattern. a) PL images of a preD-PP positive photopattern at different stages of development (developed using light of 470 nm, 34 mW). All scale bars are 50 µm. b) Intensity of the protected and developed regions of the photopattern and c) the corresponding intensity contrast for different development times.

light exposure the intensity contrast decreases in magnitude since the negative regions of the pattern enter their PL recovery stage while the positive regions of the pattern enter their PL decay stage (6 s panel). Eventually these shifts cause the intensity contrast to reach a zero value (12 s panel) which makes the photopattern difficult to observe. Continued light exposure after this point leads to the emergence of a positive contrast (17 s panel). The pattern contrast stabilizes once all regions of the pattern enter the linear portion of their PL recovery stage since there is a near constant difference of intensity (59 s panel).

PL cross sections, intensity tracking, and intensity contrast determination at different stages of the post-exposure period show a clear switch from a negative IC to a positive IC after 59 s of post exposure (Figure 8b–d). It is worth noting that the magnitude of intensity contrast is greater for the negative photopattern than for the positive photopattern. This asymmetry of pattern contrast stems from the large difference of rate between the decay step (seconds) and the recovery step (minutes), as made clear by the logarithmic timescale (Figure 1b). When the negative photopattern is exposed to light, the high-intensity regions undergo a rapid decay while the low-intensity regions undergo a slow recovery. In other words, the high-intensity regions (which are decaying) "catch up" to the low-intensity regions (which are recovering). Because this contrast asymmetry is intrinsically linked to the relative magnitude of the decay and recovery rates, it could be minimized if the decay and recovery rates were equalized (potentially through QD composition engineering). The ability to switch from negative to positive intensity contrast without changing the experimental setup is unprecedented and could have interesting applications in light sensing and switching.

2.7. Photopatterning Stability (Fading and Recharging)

The unstable nature of the QD emission (which allows for the photopatterns to be fabricated) raises questions about the stability of these photopatterns after fabrication. PL imaging of a positive photopattern placed in darkness over a period of 1 d shows that the intensity and contrast of the pattern decrease continuously, leading to a faded pattern (**Figure 9**a,c).

However, the intensity and contrast of the faded photopattern can be "recharged" by continuous light exposure (Figure 9b,c). Recharging can effectively recover the intensity to near the initial value, while the pattern contrast is only partially recovered since recharging increases the intensity of both the dark and bright regions of the photopattern (Figure 9c, inset). Nearly identical fading and recharging of intensity and contrast are observed for a photopattern placed in an ambient light environment (instead of darkness) (Figure S9, Supporting Information). These results show that mechanism leading to the PL intensity recovery, which is used to create the positive photopatterns, is partially reversible and requires constant input of light to be maintained. This suggests that the recovery of PL intensity is due to a reversible dynamic process, possibly light-mediated H_2O surface passivation of the QD[38] or photo-initiated ligand rearrangement.[51]

3. General Discussion and Conclusions

In conclusion, we demonstrated that traditional core–shell CdSe/ZnS QDs exhibit a two-step decay-to-recovery behavior of PL emission under continuous light exposure, with a two orders

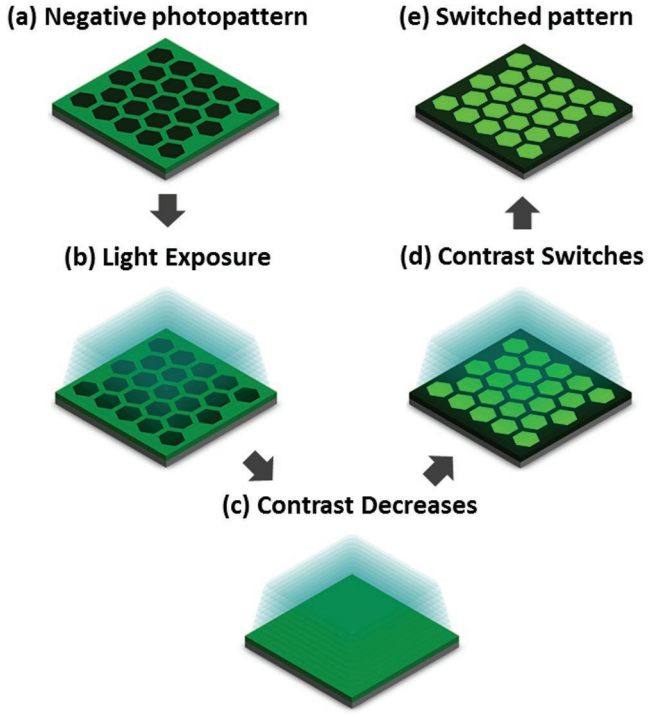

Figure 7. A photopatterning approach that can switch the contrast of the photopattern from negative to positive. a,b) This approach (negative-to-positive contrast switching, N-P-CS) involves exposing a negative photopattern to light for extended periods of time. c) The intensity contrast of the pattern decreases to a near-neutral contrast state and d) then emerges with a switched contrast (dark-to-bright and bright-to-dark) with continued light exposure. e) In the end, the photopattern has an intensity contrast that is opposite to the original contrast.

of magnitude difference in the rate of these steps (seconds vs minutes) that can be efficiently exploited for facile PL patterning. The two-step decay-to-recovery behavior of the unstable CdSe/ZnS QDs makes possible novel photopatterning strategies for creating a variety of photopatterns (negative, positive, preliminary-decay positive, and negative-to-positive contrast switching), significantly extending the capability to spatially manipulate the emissive properties of PL materials. These photopatterning strategies are analogous to traditional positive and negative patterning in electron/photolithography, a first in the area of photopatterning, and represent a noteworthy development in the area of photonics. Furthermore, the four different photopatterning approaches considerably extend the field of PL photopatterning by reducing pattern development time by a factor of 100–10 000 (from hours to seconds) while maintaining spatial resolution. Finally, the most striking feature is the ability to continuously convert from a negative to a positive photopattern using simple light exposure.

The comparison of the four outlined photopatterning approaches in terms of the required development time, pattern contrast, complexity, and pattern stability are outlined in **Table 1**.

The variety of approaches and the range of advantages and disadvantages of each approach provide a great degree of flexibility in terms of pattern development, vastly increasing the potential applications. For example, microscale optical sensors could be developed where the response time of the system is controlled by utilizing either the decay step (responds in seconds) or the recovery step (responds over many minutes). Furthermore, these approaches can be combined by successively developing the same areas of a film using different

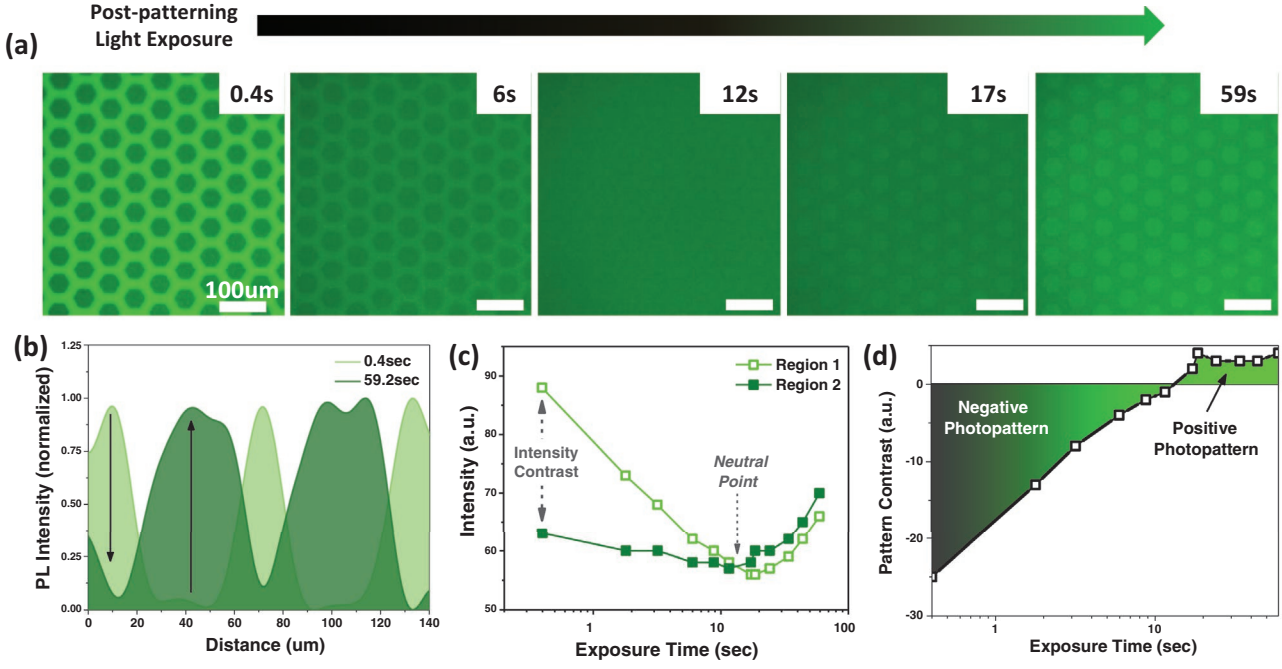

Figure 8. Negative-to-positive contrast switching (N-P-CS) occurs by exposing a negative photopattern to light for extended periods of time (470 nm, 23 mW). a) PL imaging of the photopattern during different stages of the post exposure. b) Cross section of the photopattern at the beginning (0.4 s) and toward the end (59 s) of post exposure, demonstrating the switch of photopattern contrast (negative-to-positive). c) Intensity of the different regions of the photopattern and d) the corresponding intensity contrast. All scale bars are 100 µm.

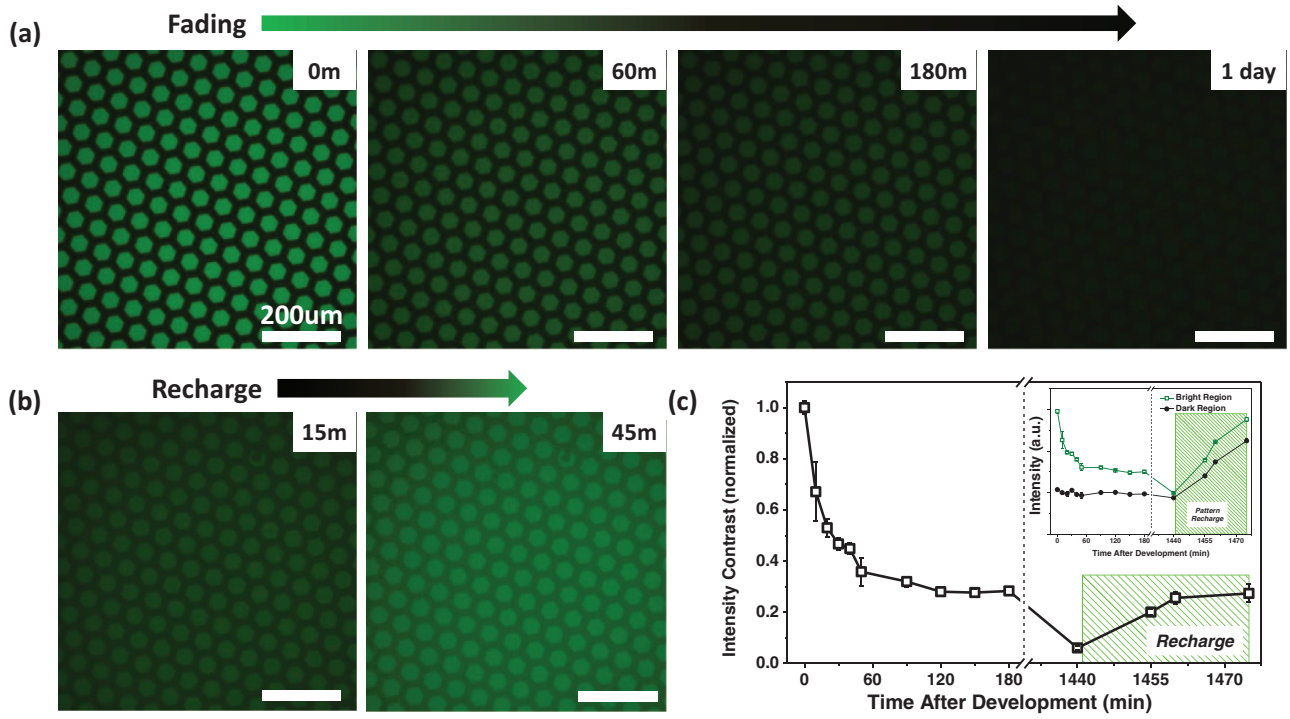

Figure 9. The unstable nature of the QD emission (which allows for photopatterns to be fabricated) also causes the pattern contrast to fade over time. a) PL imaging of a positive photopattern over a period of 1 d (in darkness) demonstrating the fading behavior. b) PL imaging of the same (1 d old) photopattern after being recharged by light exposure for 15 and 45 min (470 nm). c) Evolution of the intensity contrast of the positive pattern (normalized to initial value). (Inset) The intensity of the bright and dark regions of the pattern over the same period of time. All scale bars are 200 µm.

photopatterning approaches to create complex spatial and spectral patterns that may not be possible using other traditional lithographic patterning approaches. In addition, the outlined approaches are general, being compatible with other materials like conjugated polymers and dyes as long as their emission changes in response to light. Finally, these results have important implications in the development of nano/microscale photonic patterns over macroscopic lateral areas, a significant obstacle facing microscale technologies.

These strategies offer significant new capabilities in the areas of photonic-based anti-counterfeiting labels, light sensors, and display technology where control of emission wavelength, spatial distribution, and spatial resolution is critical. In addition, photopatterning could be revolutionary in the area of parity-time optical systems, which require optical gain-loss contrast with minimal modulation of the real refractive index.

Naturally, a number of challenges should be overcome to facilitate the implementation of photopatterning in areas like anti-counterfeiting and parity-time systems.[24] The primary obstacle is how to "lock-in" the QD photopattern after its development. Although it was shown that the intensity and contrast of older faded photopatterns can be "recharged" by simple light exposure, there are instances where this approach may not be appropriate. Possible options for pattern "lock-in" include more elaborate QD architectures, or more likely, the deposition of cladding films that prohibit the diffusion of gases (like oxygen) into the film that are thought to play a critical role in the evolution of PL intensity upon light exposure.

4. Experimental Section

Chemicals and Materials: Cadmium oxide (CdO), tri-*n*-octylphosphine (TOP, 90%), tributylphosphine (TBP, >93.5%), and poly(methyl methacrylate) (PMMA) (M_W = 120000) were obtained from Sigma Aldrich. Selenium powder (Se, 99.999%), 1-tetradecylphosphonic acid (TDPA, 98%), tri-*n*-octylphosphine oxide (TOPO, 90%), diethylzinc (15 wt% in hexane), and hexane were obtained from Alfa Aesar. Hexadecylamine (HDA, 90%) and bis(trimethylsilyl) sulfide (95%) were obtained from TCI. Toluene was obtained from BDH Chemicals. All chemicals were used as received.

Table 1. Comparison of the four outlined photopatterning techniques and the advantages and disadvantages associated with each technique.

Approach	Intensity Contrast	Advantages	Disadvantages
Negative (NP)	Negative	Fast development (sec), high contrast	Poor pattern stability
Positive (PP)	Positive	Moderate pattern stability, high contrast	Longer development (min)
Pre-decay positive (preD-PP)	Positive	Good pattern stability, high contrast	Longer development (min), requires two-steps
Neg-to-pos contrast switching (N-P-CS)	Negative-to-positive	Switchable intensity contrast, high negative contrast	Requires post-exposure, low positive contrast

Synthesis, Unstable Green CdSe/ZnS QDs: Green-emitting CdSe QDs were synthesized following a literature procedure.[12,33] Initially, 50 mg of CdO, 300 mg of TDPA, and 4 g of TOPO were inserted into a three-neck flask. The mixture was heated to 120 °C and degassed for 1 h. Subsequently, the temperature was increased to 290 °C under argon. After the solution became clear and transparent, 1 mL of 1 M Se/TBP solution was quickly injected in order to initiate nucleation and growth. CdSe QDs were grown at 290 °C for 10 s. The heating mantle was then removed to stop the reaction. Afterward, once the temperature reached 70 °C, 5 mL of hexane was added to the solution.

The ZnS shell for the unstable CdSe/ZnS core/shell QDs was synthesized following a procedure reported in literature.[14,33] Initially, 2 g of TOPO and 1 g of HDA were inserted into a three-neck flask and degassed at 120 °C for 1 h. Afterward, 5 mL of CdSe core QDs were added and the temperature was increased to 220 °C under Argon. Following this, precursor solution (0.15 mL of diethylzinc and 0.05 mL of bis(trimethylsilyl) sulfide in 1 mL of trioctylphosphine) was injected dropwise to the vigorously stirring reaction mixture. The reaction proceeded for 30 min to grow the ZnS shell. The heating mantle was then removed to stop reaction. 5 mL of hexane was added to the solution once the temperature reached 70 °C.

Sample Preparation: QD-polymer films of thickness 350 nm (±90 nm) (as evaluated by ellipsometry) were prepared by spin-casting a QD-polymer mixture at 2000–2500 rpm for 1–1.5 min, as outlined in a previous publication.[33] Films typically films had a QD-loading of ≈1% volume fraction, which was estimated via fitting of refractive indices derived from ellipsometry data with the Bruggeman model.[52] The QD-polymer mixture was made by mixing equal parts of a QD toluene solution with a 10%–12% PMMA toluene solution, and then vortexing. Films were deposited on silicon with a 290–295 nm surface layer of SiO_2.

Photomask and Photopattern Development: The photomask was a hexagonal mesh (G400H-Cu grid) TEM grid from Electron Microscopy Sciences. The TEM grid was designed to have a pitch of 62 μm, holes of 37 μm, and bars of 25 μm. Photopatterning development was performed using a 10× objective (NA: 0.30) with excitation light of 450–490 nm light over a range of powers, as outlined in a previous publication.[33] The light source was a 120 W Hg vapor short arc lamp (X-cite series, 120Q, Lumen Dynamics) with controllable power output.

Characterization: The photoluminescence spectra and time evolution of the QD-polymer films were determined from hyperspectral datacubes, which were collected using a CytoViva Hyperspectral scanning system using a diffraction grating spectrophotometer (spectral range of 400–1000 nm). The evolution of the PL intensity of the CdSe/ZnS QDs was examined under continuous light exposure (470 nm) over a period of 45 min. A 10× objective (NA: 0.30) was used during scanning (scan sizes varied). A 0.25 s exposure time (per line) was used for most scans. Hyperspectral scans were conducted using the blue excitation bandpass filter (450–490 nm) setup already mentioned. The light source was the 120 W Hg vapor short arc lamp, X-cite series, 120Q, Lumen Dynamics. Fast decay dynamics were calculated by treating each line of a hyperspectral data cube as a time point (≈650 points per line were averaged). A Savitzky–Golay filter was applied in some instances to reduce high-frequency noise.

Photoluminescence, dark field, and bright field images were collected with a cooled Dagexcel-M Digital Firewire camera and a 10× objective (NA: 0.30), as outlined in a previous work.[33] All photoluminescence imaging was performed using optical excitation from a blue bandpass filter (450–490 nm) with a dichroic mirror that reflects optical wavelengths below 495 nm and with a longpass emission filter that passes optical wavelengths above 500 nm. The light source was a 120 W Hg vapor short arc lamp (X-cite series, 120Q, Lumen Dynamics) with controllable power output. The PL cross sections and intensity of different regions of a photopattern were obtained using the "plot profile" capabilities of the ImageJ software (1.48v). The size of the image was specified by inputting known pixel μm^{-1} scaling from the Dagexcel-M Digital Firewire camera.

The thickness of the QD-polymer films was measured using a spectroscopic ellipsometer (Woollam, model M2000) with a wavelength range of 245–1000 nm and a rotating compensator configuration. Film thickness was determined by applying a Cauchy model to the 620–1000 nm (near-transparent) region of the optical spectrum, as outlined previously.[33]

AFM scans (topographical and phase) were collected with a Dimension Icon AFM microscope (Bruker) in tapping mode according to previously outlined procedures.[53] MikroMasch Si tips were used (height: 15 μm, cantilever length: 150 μm, spring constant: 7 N m^{-1}). AFM scans typically had a size of 60 μm × 60 um with a scan rate within 0.3–0.8 Hz.

Supporting Information

Supporting Information is available from the Wiley Online Library or from the author.

Acknowledgements

Financial support is acknowledged from the Air Force Office of Scientific Research FA9550-14-1-0037 (synthetic photonics multidisciplinary university research initiative, synthesis, fabrication, and development). M. J. Smith would like to acknowledge the Science, Mathematics, and Research for Transformation (SMART) scholarship funded by Office of Secretary Defense-Test and Evaluation (OSD-T&E), Defense-Wide/PE0601120D8Z National Defense Education Program (NDEP)/BA-1, Basic Research, SMART Program office Grant No. N00244-09-1-0081.

Received: June 30, 2016
Revised: August 11, 2016
Published online: September 22, 2016

[1] D. V. Talapin, J. S. Lee, M. V. Kovalenko, E. V. Shevchenko, *Chem. Rev.* **2010**, *110*, 389.
[2] N. L. Rosi, C. A. Mirkin, *Chem. Rev.* **2005**, *105*, 1547.
[3] H. Ko, S. Singamaneni, V. V. Tsukruk, *Small* **2008**, *4*, 1576.
[4] Y. N. Xia, P. D. Yang, Y. G. Sun, Y. Y. Wu, B. Mayers, B. Gates, Y. D. Yin, F. Kim, Y. Q. Yan, *Adv. Mater.* **2003**, *15*, 353.
[5] C. Hanske, M. Tebbe, C. Kuttner, V. Bieber, V. V. Tsukruk, M. Chanana, T. A. F. Konig, A. Fery, *Nano Lett.* **2014**, *14*, 6863.
[6] X. Huang, I. H. El-Sayed, W. Qian, M. A. El-Sayed, *J. Am. Chem. Soc.* **2006**, *128*, 2115.
[7] N. Gandra, A. Abbas, L. Tian, S. Singamaneni, *Nano Lett.* **2012**, *12*, 2645.
[8] R. Geryak, J. Geldmeier, K. Wallace, V. V. Tsukruk, *Nano Lett.* **2015**, *15*, 2679.
[9] A. M. Kapitonov, A. P. Stupak, S. V. Gaponenko, E. P. Petrov, A. L. Rogach, A. Eychmuller, *J. Phys. Chem. B* **1999**, *103*, 10109.
[10] K. F. Lin, H. M. Cheng, H. C. Hsu, L. J. Lin, W. F. Hsieh, *Chem. Phys. Lett.* **2005**, *409*, 208.
[11] N. Gaponik, S. G. Hickey, D. Dorfs, A. L. Rogach, A. Eychmüller, *Small* **2010**, *6*, 1364.
[12] Z. A. Peng, X. G. Peng, *J. Am. Chem. Soc.* **2001**, *123*, 183.
[13] H. Y. Qin, Y. Niu, R. Y. Meng, X. Lin, R. C. Lai, W. Fang, X. G. Peng, *J. Am. Chem. Soc.* **2014**, *136*, 179.
[14] B. O. Dabbousi, J. RodriguezViejo, F. V. Mikulec, J. R. Heine, H. Mattoussi, R. Ober, K. F. Jensen, M. G. Bawendi, *J. Phys. Chem. B* **1997**, *101*, 9463.
[15] J. Jung, C. H. Lin, Y. J. Yoon, S. T. Malak, Y. Zhai, E. L. Thomas, V. Vardeny, V. V. Tsukruk, Z. Lin, *Angew. Chem., Int. Ed.* **2016**, *55*, 5071.

[16] D. V. Talapin, I. Mekis, S. Götzinger, A. Kornowski, O. Benson, H. Weller, *J. Phys. Chem. B* **2004**, *108*, 18826.
[17] I. L. Medintz, H. T. Uyeda, E. R. Goldman, H. Mattoussi, *Nat. Mater.* **2005**, *4*, 435.
[18] B. S. Mashford, M. Stevenson, Z. Popovic, C. Hamilton, Z. Q. Zhou, C. Breen, J. Steckel, V. Bulovic, M. Bawendi, S. Coe-Sullivan, P. T. Kazlas, *Nat. Photonics* **2013**, *7*, 407.
[19] M. Gratzel, *Inorg. Chem.* **2005**, *44*, 6841.
[20] P. V. Kamat, *J. Phys. Chem. C* **2008**, *112*, 18737.
[21] H.-A. Engel, D. Loss, *Science* **2005**, *309*, 586.
[22] C. Dang, J. Lee, C. Breen, J. S. Steckel, S. Coe-Sullivan, A. Nurmikko, *Nat. Nanotechnol.* **2012**, *7*, 335.
[23] V. I. Klimov, S. A. Ivanov, J. Nanda, M. Achermann, I. Bezel, J. A. McGuire, A. Piryatinski, *Nature* **2007**, *447*, 441.
[24] C. H. Lin, E. Lafalce, J. Jung, M. J. Smith, S. T. Malak, S. Aryal, Y. J. Yoon, Y. Zhai, Z. Lin, Z. V. Vardeny, V. V. Tsukruk, *ACS Photonics* **2016**, *3*, 647.
[25] A. Biswas, I. S. Bayer, A. S. Biris, T. Wang, E. Dervishi, F. Faupel, *Adv. Colloid Interface Sci.* **2012**, *170*, 2.
[26] D. Qin, Y. N. Xia, G. M. Whitesides, *Nat. Protoc.* **2010**, *5*, 491.
[27] S. L. Young, M. Gupta, C. Hanske, A. Fery, T. Scheibel, V. V. Tsukruk, *Biomacromolecules* **2012**, *13*, 3189.
[28] M. Kuang, J. Wang, B. Bao, F. Li, L. Wang, L. Jiang, Y. Song, *Adv. Opt. Mater.* **2014**, *2*, 34.
[29] B. D. Gates, Q. B. Xu, M. Stewart, D. Ryan, C. G. Willson, G. M. Whitesides, *Chem. Rev.* **2005**, *105*, 1171.
[30] M. Tagliazucchi, V. A. Amin, S. T. Schneebeli, J. F. Stoddart, E. A. Weiss, *Adv. Mater.* **2012**, *24*, 3617.
[31] Y. Wang, Z. Y. Tang, M. A. Correa-Duarte, L. M. Liz-Marzan, N. A. Kotov, *J. Am. Chem. Soc.* **2003**, *125*, 2830.
[32] J. Chen, Y.-H. Chan, T. Yang, S. E. Wark, D. H. Son, J. D. Batteas, *J. Am. Chem. Soc.* **2009**, *131*, 18204.
[33] S. T. Malak, J. Jung, Y. J. Yoon, M. J. Smith, C. H. Lin, Z. Lin, V. V. Tsukruk, *Adv. Opt. Mater.* **2016**, *4*, 608.
[34] M. A. Miri, A. Regensburger, U. Peschel, D. N. Christodoulides, *Phys. Rev. A* **2012**, *86*, 023807.
[35] A. Regensburger, C. Bersch, M. A. Miri, G. Onishchukov, D. N. Christodoulides, U. Peschel, *Nature* **2012**, *488*, 167.
[36] T. Uematsu, J. Kimura, Y. Yamaguchi, *Nanotechnology* **2004**, *15*, 822.
[37] K. Pechstedt, T. Whittle, J. Baumberg, T. Melvin, *J. Phys. Chem. C* **2010**, *114*, 12069.
[38] A. Y. Nazzal, X. Y. Wang, L. H. Qu, W. Yu, Y. J. Wang, X. G. Peng, M. Xiao, *J. Phys. Chem. B* **2004**, *108*, 5507.
[39] S. R. Cordero, P. J. Carson, R. A. Estabrook, G. F. Strouse, S. K. Buratto, *J. Phys. Chem. B* **2000**, *104*, 12137.
[40] J. Kimura, T. Uematsu, S. Maenosono, Y. Yamaguchi, *J. Phys. Chem. B* **2004**, *108*, 13258.
[41] M. Shinya, D. C. Danov, S. Soichiro, Y. Yukio, *Jpn. J. Appl. Phys.* **2000**, *39*, 4006.
[42] S. Maenosono, *Chem. Phys. Lett.* **2003**, *376*, 666.
[43] D. Zimnitsky, C. Jiang, J. Xu, Z. Lin, V. V. Tsukruk, *Langmuir* **2007**, *23*, 4509.
[44] D. Zimnitsky, C. Jiang, J. Xu, Z. Lin, L. Zhang, V. V. Tsukruk, *Langmuir* **2007**, *23*, 10176.
[45] A. B. Greytak, P. M. Allen, W. Liu, J. Zhao, E. R. Young, Z. Popovic, B. J. Walker, D. G. Nocera, M. G. Bawendi, *Chem. Sci.* **2012**, *3*, 2028.
[46] K. Gong, D. F. Kelley, *J. Phys. Chem. Lett.* **2015**, *6*, 1559.
[47] A. M. Smith, A. M. Mohs, S. Nie, *Nat. Nanotechnol.* **2009**, *4*, 56.
[48] W. van Sark, P. Frederix, D. J. Van den Heuvel, H. C. Gerritsen, A. A. Bol, J. N. J. van Lingen, C. D. Donega, A. Meijerink, *J. Phys. Chem. B* **2001**, *105*, 8281.
[49] Y. Wang, Z. Tang, M. A. Correa-Duarte, I. Pastoriza-Santos, M. Giersig, N. A. Kotov, L. M. Liz-Marzán, *J. Phys. Chem. B* **2004**, *108*, 15461.
[50] G. A. Beane, K. Gong, D. F. Kelley, *ACS Nano* **2016**, *10*, 3755.
[51] M. Jones, J. Nedeljkovic, R. J. Ellingson, A. J. Nozik, G. Rumbles, *J. Phys. Chem. B* **2003**, *107*, 11346.
[52] *A Short Course in Ellipsometry*, J. A. Woollam Co. Inc., Lincoln, NE, USA **2010**, Ch. 2.
[53] M. E. McConney, S. Singamaneni, V. V. Tsukruk, *Polym. Rev.* **2010**, *50*, 235.